Batteries & Supercaps

Research Article
doi.org/10.1002/batt.202300158

Chemistry Europe
European Chemical Societies Publishing

www.batteries-supercaps.org

Construction of Zinc-based Anodes for Electrolytic Zinc-MnO_2 Batteries with High Discharge Voltage and Good Durability

Lexuan Yang,[a] Lijun Meng,[a] Xu Ji,[b] and Shuang Cheng*[a]

Rechargeable aqueous zinc-MnO_2 batteries have attracted great attention owing to their advantages on safety, power density, and cost. In strong acidic environment, the capacity of MnO_2-based cathode can reach 616 mAh g^{-1} through a two-electrons-transfer process of $Mn^{2+} \leftrightarrow MnO_2$. However, in acidic environment, Zn corrosion, dendrites, and hydrogen evolution reaction (HER) on the anode are rather serious, resulting in low Columbic efficiency (CE) and poor durability. Towards these issues, ZnO with dual-protection, including C and polyvinyl alcohol (PVA) coating (ZnO@C-PVA), is developed as initial anode material herein. Compared with bare CC, ZnO, and ZnO@C, reversibility of the ZnO@C-PVA electrode is largely enhanced. CE of an electrolytic full system using ZnO@C-PVA as anode and bare carbon cloth (CC) as cathode can be as high as 90% at 5 mA cm^{-2}, and discharge voltage is up to 1.85 V (mid-value), which can be maintained for 1,600 cycles, indicating rather good stability. It is believed that the existence of initial ZnO can tune the local pH around the anode, resulting in the decrease of HER and the enhancement of Zn plating. Besides, corrosion and Zn dendrites also can be inhibited effectively by the PVA layer.

Introduction

With the increasing depletion of traditional fossil energy sources and the exacerbating of related environmental problems, the need for renewable and clean energy sources is more and more urgent.[1] To realize their state grid connection, developing large-scale and efficient electrochemical storage devices, represented by rechargeable batteries, is the key link.[2] At present, lithium-ion batteries (LIBs) are the most popular ones, which have been widely used in various fields, from portable electronics to electric vehicles.[3] However, safety issue of the LIBs is serious, and fire or even explosion accidents are frequent owing to the using of organic electrolytes. Meanwhile, the costs of LIBs concerning raw materials are fast increasing. New energy storage systems with high safety and low cost as well as good environmental compatibility are urgently needed.[4]

Rechargeable aqueous batteries, using non-flammable water-based electrolytes and sustainable electrodes, have attracted the interest of numerous researchers.[5] Among in, Zn-based batteries (ZBBs) have regained widest attention due to their low cost and eco-friendly property accompanied by impressive electrochemical performance,[6] which relies on the multiple advantages of Zn-based anodes, mainly including high theoretical capacity (820 mAh g^{-1} and 5855 mAh cm^{-3} for metallic Zn), low redox potential (−0.76 V vs. SHE), high abundance (about 300 times higher than Li), and low sensitivity to oxygen and moist atmospheres.[7,8] However, although Zn is relatively inert in aqueous electrolytes, its corrosion or dissolution still cannot be completely avoided, even in mild environments.[9] Besides, hydrogen evolution reaction (HER) and Zn dendrites are also un-ignorable almost in all of the water-contained environments.[10]

As one type of typical ZBBs, alkaline Ni–Zn batteries using strong alkaline solutions as electrolytes are the first developed ones with long history of more than 150 years. Yet, they have not been widely developed owing to the low utilization of anode materials and poor stability of the cells till today.[11] Early in 1980, alkaline electrolyte was replaced by $ZnSO_4$ solution, and a reversible cycle of about 30 turns was achieved.[12] The use of mild acidic electrolyte can significantly inhibit the self-reaction of Zn, and hence improve the reversibility.[13] However, the capacities of matched cathodes that store charge through insertion/extraction mechanism, such as MnO_2 and VO_x, are always unsatisfactory. Meanwhile, the discharge potentials are relatively low, usually not higher than 1.3 V.[14] To accomplish high energy density, not only the capacity of cathodes but also the discharge potential needs to be improved. Towards this target, two or even three-chamber systems with different electrolytes to match the ideal cathode and anode, such as alkaline solution matched with Zn anode and acidic solution with MnO_2 cathode or mild solution with $LiMn_2O_4$, have been proposed, where the discharge potentials as well as the capacity of cathodes are indeed largely improved.[15,16] However, expensive and thick ion exchange membranes need to be used in these systems to separate the different electrolytes. Besides,

[a] L. Yang, L. Meng, Dr. S. Cheng
School of Environment and Energy
South China University of Technology
510006 Guangzhou (China)
E-mail: escheng@scut.edu.cn
[b] Dr. X. Ji
College of Automation
Zhongkai University of Agriculture and Engineering
510225 Guangzhou (China)

Supporting information for this article is available on the WWW under https://doi.org/10.1002/batt.202300158

Research Article
doi.org/10.1002/batt.202300158
Chemistry Europe
European Chemical Societies Publishing

the amount of total electrolyte is largely increased. And hence the total energy density is still not that high. Very recently, a new electrolytic type Zn–Mn system using strong acidic solution as electrolyte was developed, where high discharge voltage of ~1.8 V and high capacity for the cathode are achieved at the same time owing to the accomplishment of reversible reaction of Mn^{2+}/MnO_2 on the cathode (theoretical capacity of this reaction is 616 mAh g^{-1}).[17,18] Yet, the increase of H^+ leads to serious corrosion of Zn anode and the largely enhancement of HER, resulting in fast mass loss and rather low coulombic efficiency (CE) on the anode.

In acidic environment, except the reversible reaction of Zn^{2+}/Zn, the concerned side reactions on the anode are as follows:

$$Zn \leftrightarrow Zn^{2+} + 2e^- \qquad E_0 = -0.76\ V\ (vs.\ SHE\ pH \leq 7) \tag{1}$$

$$2H^+ + 2e^- \leftrightarrow 2H_2 \qquad E_0 = 0\ V\ vs.\ SHE\ (pH = 1) \tag{2}$$

In order to inhibit the side reactions and improve the stability of anode, several strategies have been proposed: 1) surface/interface modification on the anode,[19] 2) structure design of the anode, such as construction of 3D porous electrode,[20,21] 3) electrolyte optimization.[22] Specifically, TiO_2 coating realized by atomic layer deposition has be tried as protective layer on Zn plate in mild acidic electrolyte,[23] where the formation of byproduct were inhibited, and the capacity retention is up to 85% after 1000 cycles at 3 mA cm^{-2}. Zhu et al. reported a polyimide coated scheme, where a faster kinetic process and lower deposition/stripping potential were realized.[24] Recently, using acetic acid (HAc) as buffer additive, the "fluctuation" phenomenon was effectively inhibited, "self-regulation" mechanism was realized in a cathode-free Zn–MnO_2 system, and a long lifetime of 2000 cycles with a CE of 99.6% was achieved at 10 mA cm^{-2}.[25] Yet, the discharge voltage of these systems are usually low owing to the absence of strong acidic environment.

Herein, an efficient strategy that stable and high-efficiency Zn plating/stripping can be realized in strong acidic solution was developed. In this system, ZnO loaded on carbon cloth (CC) was used as initial anode, and a dual-protection strategy was conducted towards it, including C coating on the ZnO and PVA layer coating on the electrode, which is abbreviated as ZnO@C-PVA; An aqueous solution with pH = 1 was prepared as electrolyte (1 M $ZnSO_4$ + 1 M $MnCl_2$, (sulfuric acid was used to adjust the pH); Bare CC was chosen as current collector of the cathode. In a three-electrode configuration, the CE of ZnO@C-PVA is largely enhanced compared with the initial anodes using bare CC, ZnO, and ZnO@C. The CE of full cells using ZnO@C-PVA as initial anode can be as high as 90% at 5 mA cm^{-2} with a fixed areal charge capacity of 0.5 mAh cm^{-2}. Meanwhile, the discharge voltage is up to 1.85 V (mid-value). Good performance can be maintained for 1,600 cycles, indicating rather good stability.

Results and Discussion

Shown in Figure 1 is electrochemical performance of the separated single electrode in a three-electrode configuration and paired electrodes in a two-electrode system. In the CV curves with a negative potential range of −1.4–0 V shown in

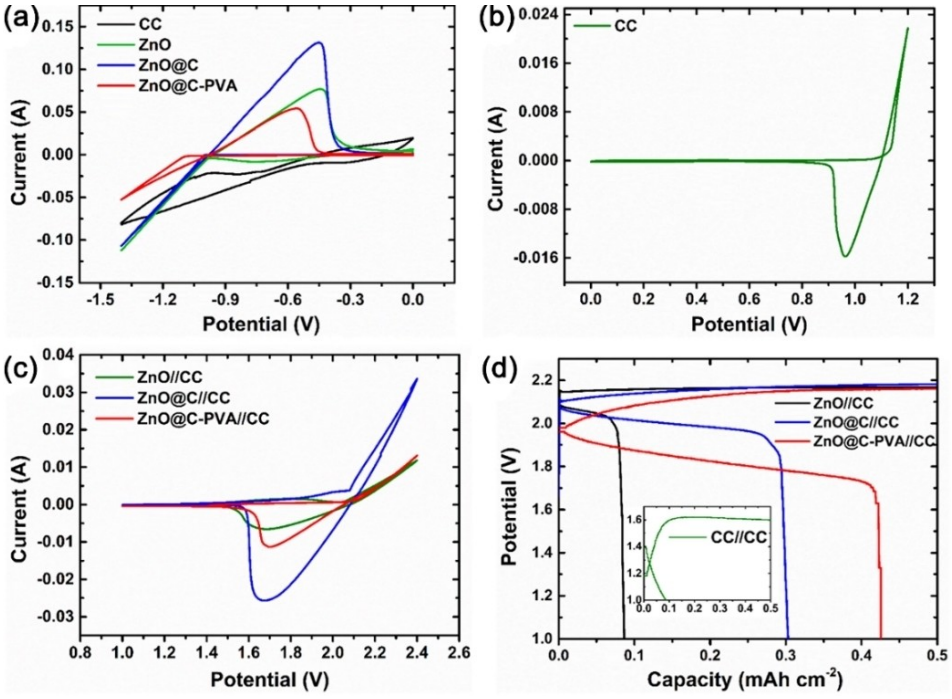

Figure 1. Electrochemical performance in a three-electrode configuration: CV curves of a) the various anodes and b) the active material-free CC cathode at a scan rate of 10 mV s^{-1}. Electrochemical performance in a two-electrode system: c) CV curves at 10 mV s^{-1} and d) GCD curves at 5 mA cm^{-2} of the three pairs.

Figure 1(a), obvious redox pair that corresponding to the plating/stripping of Zn can be observed for the three electrodes loaded with ZnO-based materials, ZnO, ZnO@C and ZnO@C-PVA, while no redox pair can be observed for the bare CC at identical test condition, suggesting that HER can be inhibited on the three ZnO-based electrodes. Compared with that of the ZnO@C and the ZnO@C-PVA, the ratio of anodic/cathodic peek of the ZnO electrode is obviously smaller, reflecting larger proportion of HER during cathodic sweep. At an identical sweep rate of 10 mV s^{-1}, reaction reversibility of the ZnO@C and the ZnO@C-PVA is similar, while the response current of the ZnO@C is much larger than that of the later, implying higher conductivity of the ZnO@C. From the above results, it can be concluded that the existence of ZnO can inhibit the HER effectively, which should be attributed to the influence on local pH of the ZnO. However, ZnO is unconductive semi-conductor and is not stable in acidic solution, therefore its influence is time-limited. The covering of C can not only protect the ZnO but also improve the conductivity. The PVA layer can further enhance this protection, while it will induce the decrease of ionic conductivity and hence the decrease of response current.

In a positive potential range, bare CC was used as active material-free cathode electrode. Shown in Figure 1(b), an obvious redox pair at a rather high potential range of ~1.0 V vs. Ag/AgCl can be observed, suggesting the existence of reversible Mn^{2+}/MnO_2 reaction. Meanwhile, it can be seen that the anodic peak is slightly higher than the cathodic peak, implying that there are also some irreversible side reactions.

Brief CV and GCD curves of the CC//CC, ZnO//CC, ZnO@C//CC, and ZnO@C-PVA//CC pairs were then collected and presented in Figure 1(c and d). There is no redox pair for the active materials-free pair of CC//CC in the CV curve, and hence it is not presented in Figure 1(c). While obvious redox pairs with cathodic peaks at about 1.7 V can be observed in the CV curves of all the other pairs. The ZnO@C//CC pair exhibits the largest current response. Yet, its anodic peak is obviously larger than the cathodic peak, reflecting limited reversibility. The ZnO//CC pair shows the smallest current response together with lowest reversibility. For the ZnO@C-PVA//CC pair with PVA coated on the electrode, though its current response is not that high compared with that of the ZnO@C//CC, reversibility of its redox pair is obvious higher, implying unenergetic side reactions on the anode, mainly including self-dissolution of Zn plated on and HER, which can be further inhibited by the protection of PVA layer, even in strong acidic environment. Correspondingly, in the GCD curves with a current density of 5 mA cm^{-2} and a fixed charge capacity of 0.5 mAh cm^{-2}, the CC//CC pair has no obvious discharge platform (inset of Figure 1d), while long plateaus can be observed for the other three pairs. Discharge voltages of the three cells are rather high, up to 1.8–2.0 V. Yet, discharge capacities of the ZnO//CC and ZnO@C//CC are relatively low, corresponding to CEs of about 16.0% and 66.7%, respectively. For the ZnO@C-PVA//CC electrode pair, though its discharge voltage is relatively low, with a mid-value of ~1.8 V, it possesses the longest discharge plateau, corresponding to a CE of ~85.0%.

It can be seen that though all the initial anodes are Zn-free, HER can be inhibited owing to the existence of ZnO-based initial materials. For the ZnO@C electrode, the proportion of HER is lower than that of the ZnO electrode; After the coating of PVA, the HER can be further inhibited, and Zn^{2+}/Zn reaction can occur with high reversibility though its polarization voltage difference is slightly increased. Compared with bare CC, ZnO possesses higher over-potential for HER. It also can react with H^+ and reduce its local concentration around the anode, corresponding to the increase of local pH, which has been proved by the local pH measurement shown in Figure S1. The C coating can improve electrical conductivity of the ZnO and inhibit its rapid reaction with H^+. On this basis, the anode coated with a PVA film can further stop the direct contact between the active material and the strong acidic solution, inhibit Zn/ZnO corrosion and HER, and hence improve the CE and the stability of the anode.

Detailed electrochemical performance of separated electrodes in a three-electrode configuration is then presented in Figure 2. As can be seen in Figure 2(a and b), at low current densities of 1 and 2 mA cm^{-2}, charge/discharge plateaus are rather stable, and the discharge plateaus of the ZnO@C-PVA and ZnO@C are close to each other, about −0.96 V vs. Ag/AgCl, very close to the theoretical potential of the Zn^{2+}/Zn reaction stated in equation 1. Consist with above discussion, discharge platform of the ZnO@C-PVA is longer than that of the ZnO@C, suggesting higher reversibility. Yet, CE of the ZnO@C-PVA is still relatively low at a low current of 1 mA cm^{-2}, 75%. At higher current densities of 5 and 10 mA cm^{-2} shown in Figure 2(c and d), the CEs of the ZnO@C and ZnO@C-PVA are increased, and the CE can reach 99% at 10 mA cm^{-2} for the ZnO@C-PVA. On the contrast, discharge platforms can be observed only when the current density is higher than 5 mA cm^{-2} for the CC and the ZnO electrodes, while it is much shorter for the CC. Consisting with the results shown in Figure 1, the electrodes with ZnO as initial materials have better reversibility, while the electrode with dual-protection of C and PVA has the best reversibility though its polarization is a little bit high. To specify the influence of PVA, self-discharge measurement was conducted on the ZnO@C and ZnO@C-PVA at GCD current of 10 mA cm^{-2} in Figure S2. The Zn plated on the two electrodes are similar at 10 mA cm^{-2} (see Figure 2d). After 0.5 h's resting at charge state, discharge capacity of the ZnO@C is much smaller (0.15 mAh cm^{-2}) than that of the ZnO@C-PVA (0.34 mAh cm^{-2}), suggesting less Zn is oxidized during rest for the later. That is to say, PVA can inhibit the corrosion of Zn effectively.

Rate performance of the electrodes was then collected in Figure 2(e) with a fixed charge capacity of 0.5 mAh cm^{-2}. Though CEs of the ZnO@C-PVA are slight lower than that of the ZnO@C and ZnO at high current densities ($>=20$ mA cm^{-2}), its CEs are obvious higher at low current densities (<20 mA cm^{-2}). CEs of the ZnO and CC drop to zero when the current density is lower than 5 mA cm^{-2}, suggesting a high proportion of HER. The ZnO@C exhibits considerable CEs at all current densities. There is a phenomenon worth mentioning that the CEs/discharge capacities decrease along with the increase of current density for almost all the electrodes. It is different with

Research Article
doi.org/10.1002/batt.202300158
Chemistry Europe
European Chemical Societies Publishing

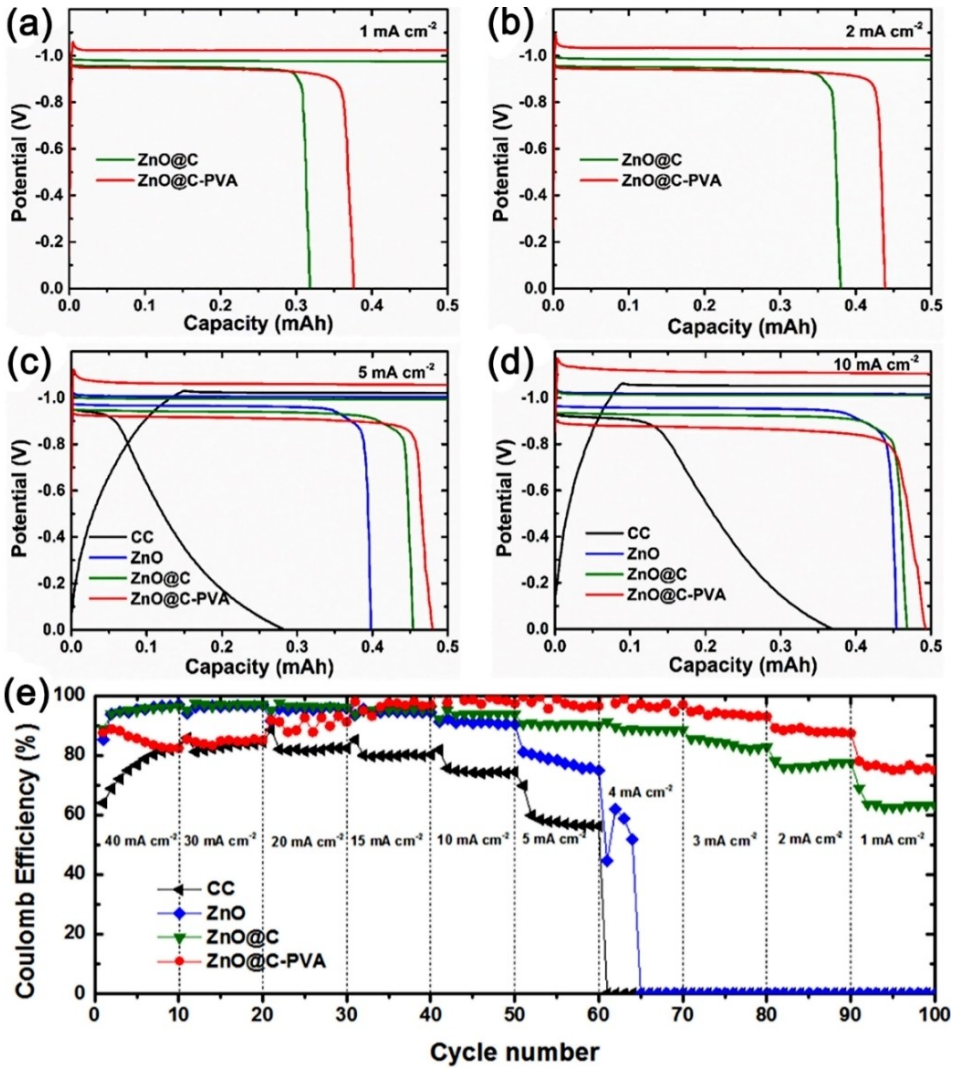

Figure 2. Detailed electrochemical performance of the various anodes in a three-electrode configuration: GCD curves at a) 1, b) 2, c) 5, and d) 10 mA cm^{-2}; e) rate performance at different current densities.

the situation observed in organic based systems, which should result from the increase of HER proportion at low current densities. As well known, charge lost concerned reactions in acidic solution are the electrochemical reduction of H^+ and the self-reaction of Zn with the H^+, which are all HER related. It is said that HER concerned side reactions decrease along with the increase of current density in aqueous systems. This phenomenon has been found in our previous reports.[26–28]

Charge storage behavior of the active-material-free cathode was then recorded in a three-electrode configuration in Figure 3. With a constant charge capacity of 0.5 mAh cm^{-2}, obvious charge/discharge plateaus can be observed at 1.1/1.0 V, shown inset of Figure 3. The potential difference between charge and discharge is small as 0.1 V. The reaction potentials, especially the discharge potentials, have negligible drop along with the increase of current density, reflecting fast reaction kinetics of the cathode. Importantly, with the increase of current density from 1 to 10 mA cm^{-2}, the discharge plateau/capacity increases, and a high CE of ~95% is achieved at 10 mA cm^{-2}, which is remained even when the current is increased to 40 mA cm^{-2}. Yet, the CEs are still below 100%, only ~83% at 1 mA cm^{-2}, which should originate from the reversible formation of Cl_2 or O_2. Similar to the change trend on anode, the CE increases along with the current density, suggesting the decrease of irreversible side reactions on the cathode. Additionally, there is only one long and stable discharge plateau, indicating that there is only one reversible reaction of Mn^{2+}/MnO_2, whose working potential is high and reaction kinetics is fast.

Charge/discharge mechanism of the cathodes and anodes were then discussed. Shown in Figure 4 is the XRD patterns and SEM images of the CC cathode at charge and discharge states. At charge state, except the XRD peaks that belong to the CC substrate, the other peaks consist well with the characteristic peaks of ε-MnO_2 (PDF#30-0820), as presented in Figure 4(a), suggesting a two-electron process of Mn^{2+} to Mn(IV)O_2 in strong acidic environment, which coincides with other reports.[29] At discharge state, there are only carbon

Research Article
doi.org/10.1002/batt.202300158
Chemistry Europe
European Chemical Societies Publishing

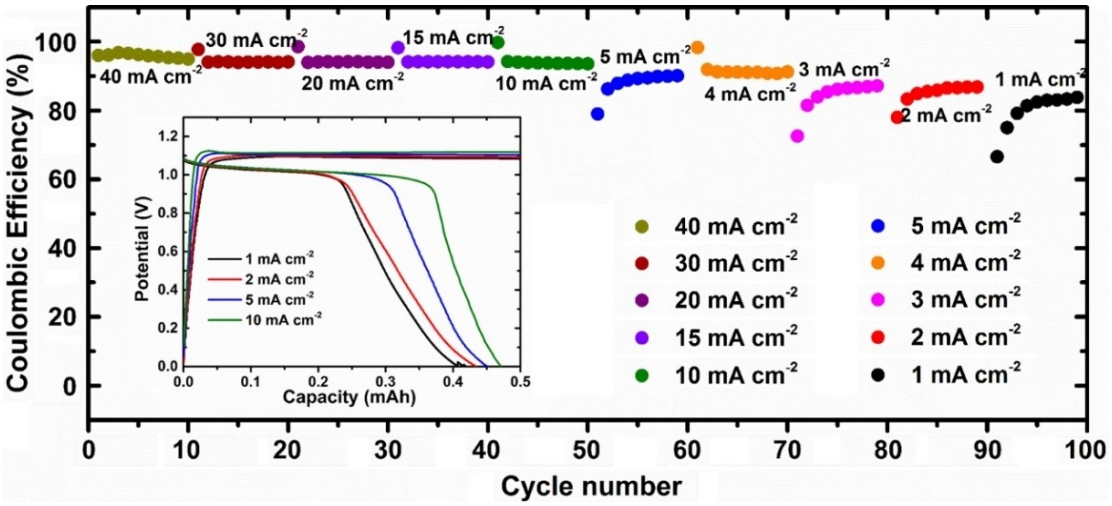

Figure 3. Rate performance of the active material-free CC cathode at various current densities, inset is the GCD curves at 1, 2, 5 and 10 mA cm^{-2}.

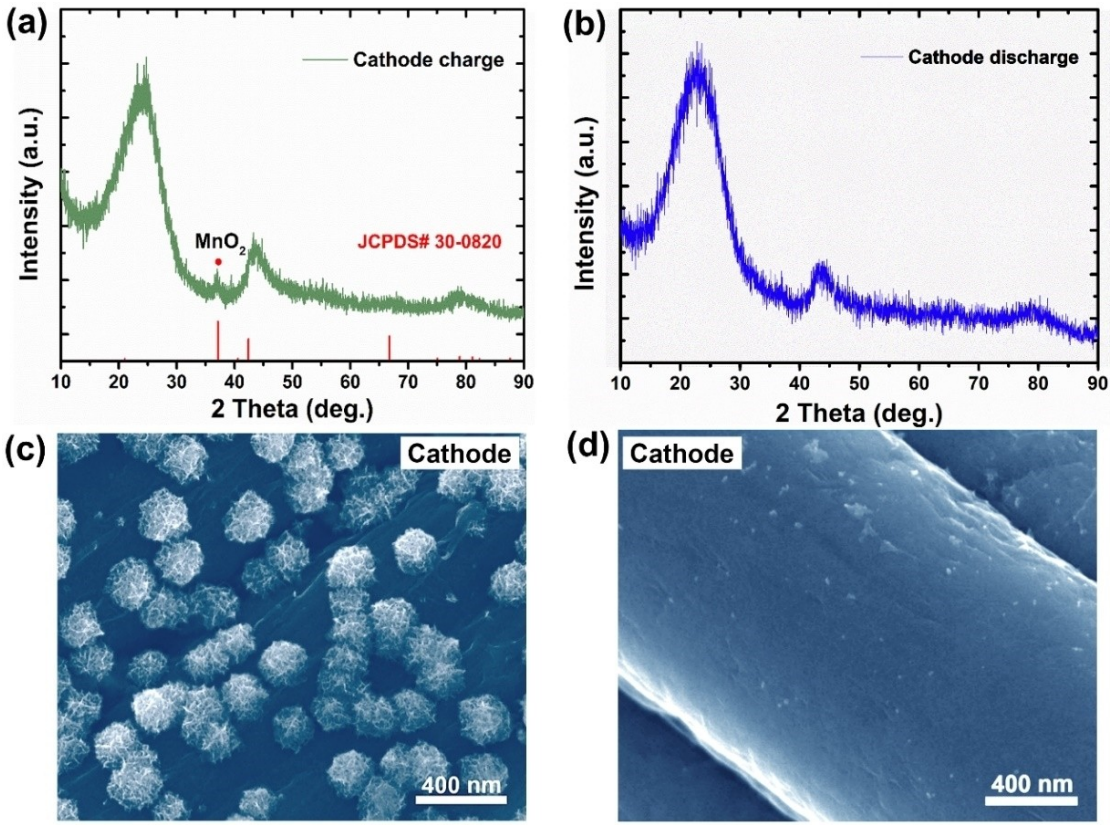

Figure 4. Structure and morphology characterization of the cathode (after 15 cycles): XRD pattern and SEM images after a), c) charging and b), d) discharging.

concerned peaks in Figure 4(b), indicating full conversion of MnO_2 to soluble Mn^{2+} during discharge process. Correspondingly, porous spheres with a diameter of ~200 nm can be observed on the surface of CC substrate at charge state, while no obvious substance is left after fully discharge, further confirming high reversibility of the Mn^{2+}/MnO_2 reaction pair.

Shown in Figure 5 is the XRD patterns and SEM images of the ZnO-based anodes at charge and discharge states. XRD patterns of the ZnO@C are presented in Figure 5(a and b). At charge state (Figure 5a), obvious characteristic peaks that belong to Zn (PDF#04-0831) can be observed, indicating a Zn plating process during charging on the anode. Meanwhile, ZnO (PDF#36-1451) concerned peaks also can be detected. At discharge state (Figure 5b), only characteristic peaks of ZnO can be detected, suggesting the stripping of Zn during discharge. The XRD results suggest a Zn/Zn^{2+} reaction process on the

Research Article
doi.org/10.1002/batt.202300158
Chemistry Europe
European Chemical Societies Publishing

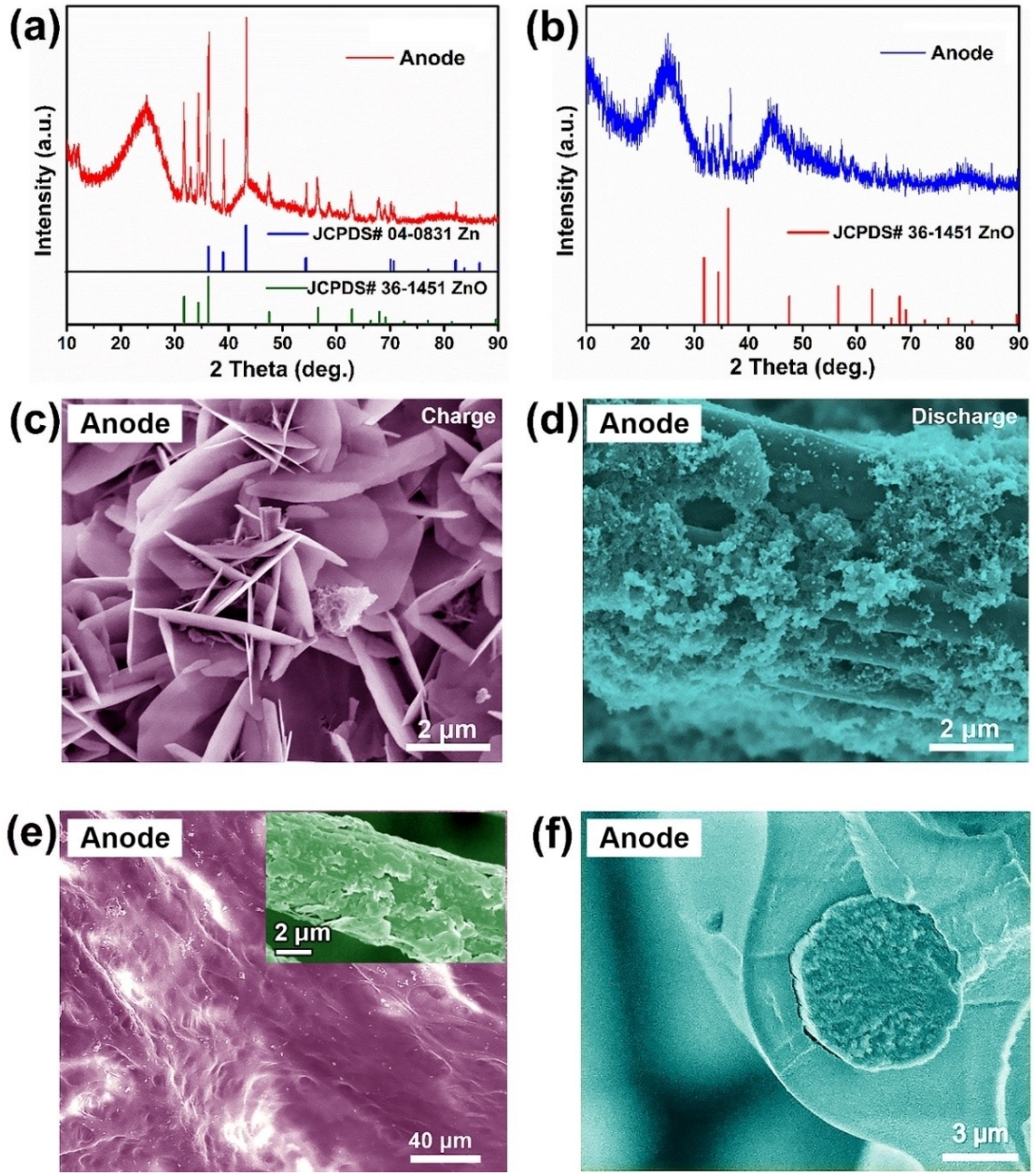

Figure 5. Morphology and phase structure characterization of the anodes (after 15 cycles): a), b) XRD patterns and c), d) SEM images of the ZnO@C electrode after charging and discharging; e), f) SEM image of the ZnO@C-PVA electrode after charging and discharging, inset is the enlarged image after the remove of PVA film.

ZnO@C anode, while the initial ZnO can be well maintained owing to the protection of C coating. The ZnO only works as active sites that Zn can be deposited on due to the high over-potential of ZnO to HER and its influence on local pH. No obvious XRD peaks can be identified for the ZnO@C/PVA anode owing to the existence of PVA layer, therefore the patterns are not shown here.

Surface morphology of the anodes was then recorded in Figure 5(c–f). It can be seen that large nano-sheets perpendicular to the surface of the carbon fiber with a size in micrometer are formed after charging, most of which exhibit hexagonal shape, characteristic shape of Zn, further indicating the deposition of Zn during charging.[30] At discharge state, only nano-particles that should be ZnO@C are left (see Figure 5d), indicating that Zn can be fully stripped, consisting with the XRD results. While, the upright growing Zn nano-sheets also can be identified the initial form of Zn dendrites, and they can induce the formation of larger Zn dendrites along cycling, which is one of the main reasons for the failure of Zn-based batteries. In other words, though reversible plating/stripping of Zn can be realized with the assistant of ZnO@C on CC, Zn dendrites cannot be fully avoided. Naturally, self-reaction of Zn is also unavoidable in this condition. SEM images of the ZnO@C-PVA after charging and discharging were also

Research Article
doi.org/10.1002/batt.202300158
Chemistry Europe
European Chemical Societies Publishing

collected in Figure 5(e and f). At charge state, only smooth surface can be seen, suggesting that Zn deposition is restricted under the PVA film. After the remove of PVA, irregular sheet structures parallel to the carbon fiber (see inset of Figure 5e) can be observed, suggesting upright growing Zn dendrites are well avoided. Moreover, as can be seen in the cross section view of one PVA coated carbon fiber (Figure 5f), thickness of the PVA layer is about 2 μm, and no sheet or dendrite-like structure can be observed all through the view. Therefore, it is safe to say that the PVA layer can not only protect the active materials from direct contact with the harsh solution but also inhibit the formation of Zn dendrites.

Electrochemical performance of the ZnO//CC, ZnO@C//CC, and ZnO@C-PVA//CC pairs was finally collected in Figure 6. With constant charge/discharge, obvious discharge plateaus can be observed for all the three pairs (Figure 6a–c), and the discharge voltage can reach 2.0 V, consisting with other electrolytic Zn-MnO_2 systems.[31] The reversible discharge capacities of the ZnO@C-PVA//CC pair are obvious higher than that of the other two pairs, and a CE of 90% can be achieved at 10 mA cm^{-2}. Yet, its discharge voltage is a little bit lower with a midpoint value of ~1.9 V, and the charge/discharge voltage difference is slightly increased along with the current density.

Similar to the above results, the discharge capacity of the electrode pairs also increases along with the current density when the current density is lower than 10 mA cm^{-2}, as shown in the rate results of Figure 6(d). At a same current density, CE (corresponding to the discharge capacity) of the ZnO@C-PVA//CC pair is obvious higher than that of the other two pairs, which should result from the higher ionic resistance and lower kinetic process of the anode owing to the existence of PVA layer. Yet, at a low current of 1 mA cm^{-2}, CE of the ZnO@C-PVA//CC pair also dramatically drops to ~42%, implying the rising of HER concerned side reactions, coinciding with above discussion. At a higher current range of 8–30 mA cm^{-2}, the CE can be well remained at about 90%, which will decrease along with the further increase of current to 40 mA cm^{-2}, suggesting electrolyte ions' kinetic process begins to dominate the CE at

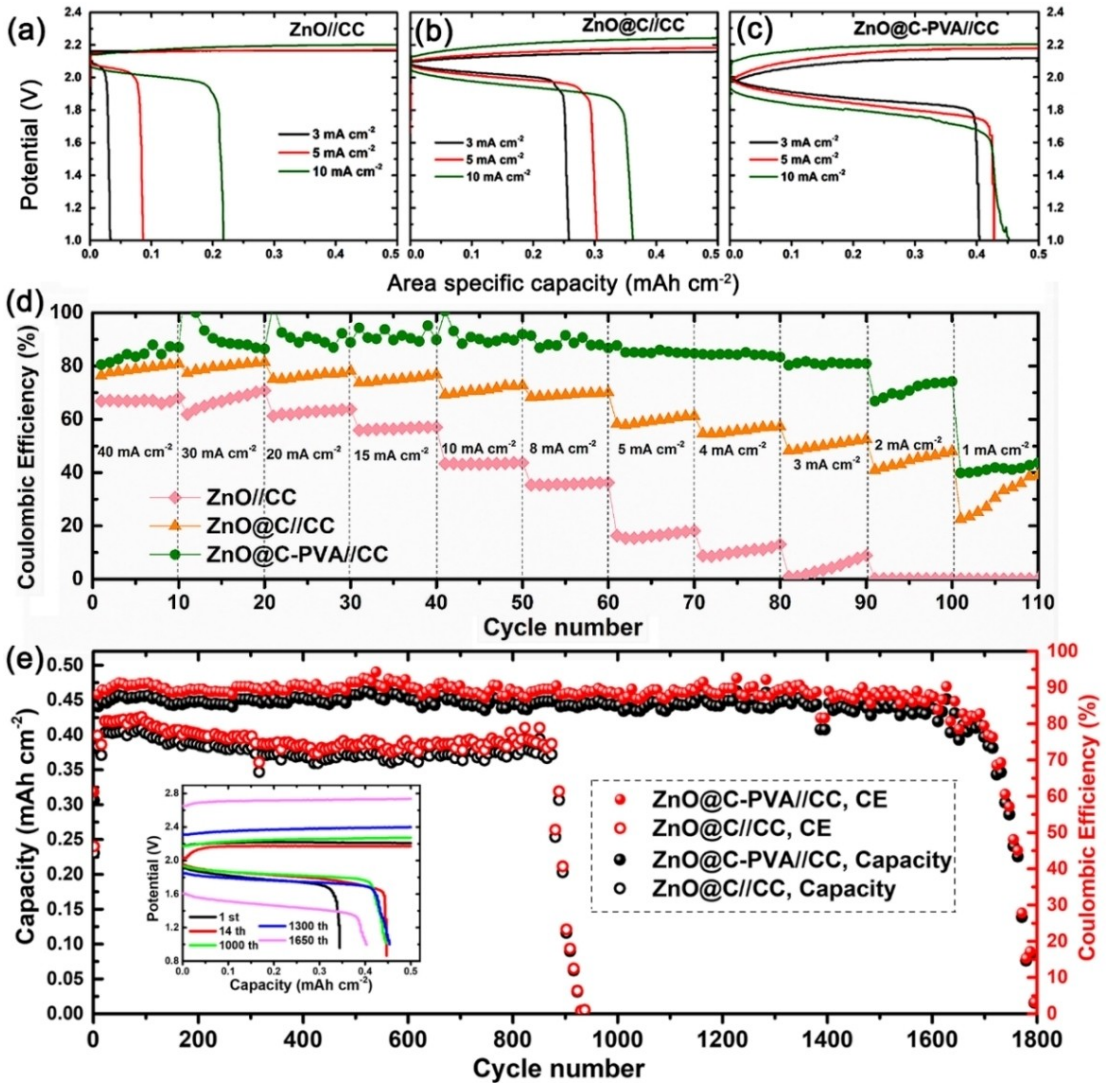

Figure 6. Electrochemical performance of the various electrode pairs: a–c) GCD curves at different current densities, d) rate performance, and e) cycling performance of the ZnO@C//CC and ZnO@C-PVA//CC pair at 5 mA cm^{-2}.

Research Article
doi.org/10.1002/batt.202300158
Chemistry Europe
European Chemical Societies Publishing

very high currents. Without the protection of C and PVA, HER concerned side reactions dominate the charge loss/CE at all current densities for the ZnO@C//CC and ZnO//CC pairs, and monotonic increase of the CE along current densities are observed, as shown in Figure 6(d).

Long-term cycling, an important index to evaluate the overall performance of a battery, of the ZnO@C//CC and ZnO@C-PVA//CC pairs was then recorded in Figure 6(e). It can be seen that though CE and discharge capacity increase obviously at the first dozen cycles for the ZnO@C//CC based system, the CE is still only ~75%, and then suddenly drops to ~0 after 880 cycles' running, which should be induced by the dissolution of ZnO active sites along cycling. In contrast, CE of the ZnO@C-PVA//CC pair remains at ~90% for 1600 cycles after initial activity. The inset of Figure 6 exhibits the discharge capacity and voltage change along cycling of the ZnO@C-PVA//CC pair. Its initial discharge capacity is 0.35 mAh cm^{-2}, corresponding to a CE of 70%, while it increases to 0.45 mAh cm^{-2} at 14th cycle and remained in the following cycles. Yet, after 1600 cycles' cycling, at 1650th cycle, the discharge capacity begins to drop accompanied by a decrease of the discharge voltage, reduced to 1.45 V from 1.85 V (mid-point value). Meanwhile, the polarization voltage (difference between charge and discharge voltage) increases obviously at 1650th cycle, suggesting that resistance increase is the main cause of fast discharge capacity/CE decay along cycling. In the system constructed here, one plausible reason of resistance increase is the structure destroy of the PVA film, which may agglomerate to bulk and stop the diffusion of Zn^{2+}; The other plausible reason is the agglomeration of less active MnO_2, whose conductivity is rather low.

XRD, Raman and SEM were then used to characterize the change of the cathode after cycling, as shown in Figure 7. Seen from the XRD pattern (Figure 7a), except the peaks that can be indexed to carbon substrate, all the other peaks can be indexed to ε-MnO_2 (PDF#30-0820), and the peak intensity is much stronger that that shown in Figure 4(a), indicating better crystallization or more substance. Consistently, ε-MnO_2 concerned bands can be observed in the Raman spectrum presented in Figure 7(b). Unlike the CC at initial charge state shown in Figure 4(c), dense and thick active materials can be found on the substrate after long-term cycling (see Figure 7c and d), suggesting excessive accumulation of ε-MnO_2 with poor conductivity, which will cause resistance increase of the system. Therefore, decreased reversibility of the ε-MnO_2 should be the main cause of discharge capacity/CE decay along cycling, which should be induced by the relative high proportion of HER concerned side reactions on the anode, leading to insufficient Zn plating/striping and hence the surplus of ε-MnO_2 in every circle since reversibility of the Mn^{2+}/MnO_2 reaction in acidic environment is usually high.

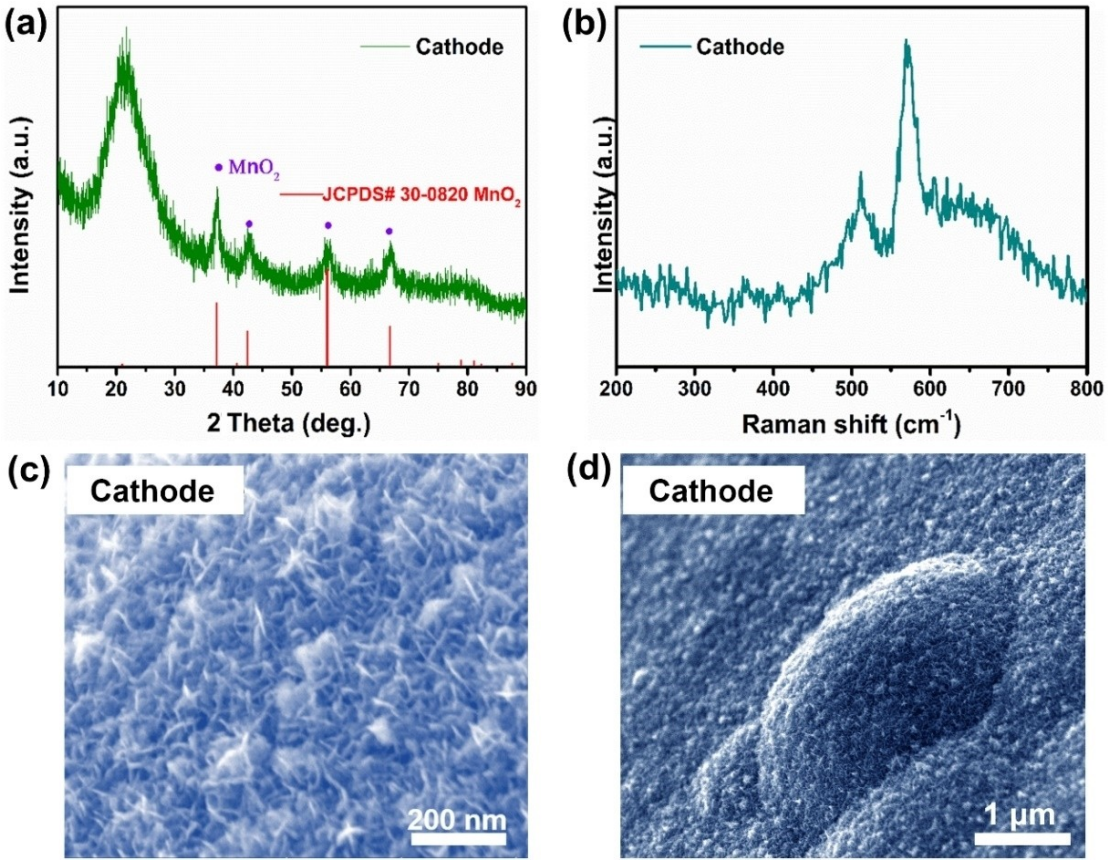

Figure 7. a) XRD pattern, b) Raman spectrum, and c), d) SEM images at different magnifications of the cathode after cycling.

Conclusions

An aqueous electrolytic Zn-MnO_2 system with high discharge voltage is developed herein. Towards the issues of Zn-based anode facing in acidic solution (pH = 1), ZnO that possesses high over-potential for HER and can increase local pH through its reaction with H^+ is used as initial material. Furthermore, a dual-protection strategy, including C and PVA layer coating, is proposed. Zn corrosion, Zn dendrites, and HER can be inhibited effectively through this strategy. Reversible and stable Zn plating/stripping is hence realized on the anode in acidic environment. Meanwhile, reversible Mn^{2+}/MnO_2 occur on the cathode. CE of the electrolytic Zn-MnO_2 system can be as high as 90% at 5 mA cm^{-2} with an area capacity of 0.5 mAh cm^{-2}. Discharge voltage is up to 1.85 V (mid-value). The good performance can be well maintained for 1,600 cycles, indicating rather good stability. The strategy proposed here is cost-effective and eco-friendly, which exhibits promising prospects in constructing aqueous batteries that can balance the energy and power density.

Experimental Section

Material preparation

The preparation method of C coated ZnO had been similarly reported in our previous work.[32] Commonly, 5.76 g oxalic acid ($H_2C_2O_4$) and zinc acetate ($C_4H_6O_4Zn$) were first mixed together and grounded for about 1 h. Then, the obtained powder was placed in a muffle furnace and heated at 450 °C for 30 min. After standing and cooling, ZnO (white powder) was obtained. Finally, C was coated onto the ZnO through co-calcination of the as-obtained ZnO powder and some phenolic substances (1 g) at 650 °C for 3 h in N_2 atmosphere.

Preparation of polyvinyl alcohol (PVA) gel: 3.5 g PVA was poured into 40 mL water under stirring and heating at a temperature of 85 °C until the solution was completely transparent. Then, 0.65 g $ZnSO_4$ was added into the solution to increase the ionic conductivity of the PVA layer.

The working electrode was prepared by mixing active material (ZnO or ZnO@C), carbon black, and polyvinylidene fluoride (PVDF) at a mass ratio of 8:1:1 in N-methyl-2-pyrrolidone (NMP) to form a slurry, which was then drizzled onto carbon cloth (CC) and dried at 80 °C in a vacuum oven. Loading amount of initial materials was controlled to be ~0.8 mg cm^{-2}. PVA coated electrode was then prepared through immersing the loaded CC into the PVA gel for about 1 min followed by drying at room temperature. The final electrode was abbreviated as ZnO@C-PVA.

Materials characterization

X-Ray diffraction (XRD) patterns of the samples were collected on a Bruker D8 Advance (Germany Bruker) equipped with a high-intensity Cu K_α irradiation (k = 1.5406 Å). Scanning electron microscopy (SEM) images were obtained using Hitachi SU8010 with a 5 kV accelerating voltage. Raman spectra were recorded on a Horiba Raman spectrophotometer (LabRAM HR Evolution, Horiba) with a wavelength of 532 nm.

Electrochemical measurements

Galvanostatic charge/discharge curves were recorded on a LAND battery cycler (CT2001 A) at room temperature. Cyclic Voltammetry (CV) was tested on a CHI660E. The related electrodes were tested in both three-electrode and two-electrode systems. In the three-electrode configuration, bare CC and Ag/AgCl were used as counter electrode and reference electrode, respectively. In the two-electrode system, electrolytic cells were constructed, where bare CC, ZnO, ZnO@C or ZnO@C-PVA was used as negative electrode separately, bare CC was used as current collector of the cathode, and a 1 M $MnCl_2$ + 1 M $ZnSO_4$ solution with a pH of 1 (adjusted with sulfuric acid) was used as electrolyte. Excessive electrolytes were used in both three-electrode and two-electrode configurations.

Acknowledgements

This work was supported by Natural Science Foundation of Guangdong Province, China (No. 2020 A1515010483).

Conflict of Interests

The authors declare no conflict of interest.

Data Availability Statement

The data that support the findings of this study are available from the corresponding author upon reasonable request.

Keywords: acidic electrolyte · dual-protection · electrolytic zinc-MnO_2 batteries · high discharge voltage · zinc-based anode

[1] S. Chu, A. Majumdar, *Nature* **2012**, *488*, 294–303.
[2] J. M. Tarascon, M. Armand, *Nature* **2001**, *414*, 359–367.
[3] T. Zhang, Y. Tang, S. Guo, X. Cao, A. Pan, G. Fang, J. Zhou, S. Liang, *Energy Environ. Sci.* **2020**, *13*, 4625–4665.
[4] J. Zhu, T. Wierzbicki, W. Li, *J. Power Sources* **2018**, *378*, 153–168.
[5] A. Bayaguud, Y. Fu, C. Zhu, *J. Energy Chem.* **2022**, *64*, 246–262.
[6] Y. Wang, Z. Wang, F. Yang, S. Liu, S. Zhang, J. Mao, Z. Guo, *Small* **2022**, *18*, 2107033.
[7] F. Wang, O. Borodin, T. Gao, X. Fan, W. Sun, F. Han, A. Faraone, J. A. Dura, K. Xu, C. Wang, *Nat. Mater.* **2018**, *17*, 543–549.
[8] S. Huang, J. Zhu, J. Tian, Z. Niu, *Chem. Eur. J.* **2019**, *25*, 14480–14494.
[9] J. Hao, X. Li, X. Zeng, D. Li, J. Mao, Z. Guo, *Energy Environ. Sci.* **2020**, *13*, 3917–3949.
[10] L. Zhang, Y. Hou, *Adv. Energy Mater.* **2021**, *11*, 2003823.
[11] H. Li, L. Ma, C. Han, Z. Wang, Z. Liu, Z. Tang, C. Zhi, *Nano Energy* **2019**, *62*, 550–587.
[12] T. Shoji, T. Yamamoto, *Electroanal. Chem.* **1993**, *362*, 153–157.
[13] J. Fu, Z. P. Cano, M. G. Park, A. Yu, M. Fowler, Z. Chen, *Adv. Mater.* **2017**, *29*, 1–34.
[14] Y. Shi, Y. Chen, L. Shi, K. Wang, B. Wang, L. Li, Y. Ma, Y. Li, Z. Sun, W. Ali, S. Ding, *Small* **2020**, *16*, 2000730.
[15] C. Zhong, B. Liu, J. Ding, X. Liu, Y. Zhong, Y. Li, C. Sun, X. Han, Y. Deng, N. Zhao, W. Hu, *Nat. Energy* **2020**, *5*, 440–449.
[16] X. Yuan, X. Wu, X.-X. Zeng, F. Wang, J. Wang, Y. Zhu, L. Fu, Y. Wu, X. Duan, *Adv. Energy Mater.* **2020**, *10*, 2001583.
[17] G. G. Yadav, D. Turney, J. Huang, X. Wei, S. Banerjee, *ACS Energy Lett.* **2019**, *4*, 2144–2146.
[18] Y. Zhu, Y. Cui, H. N. Alshareef, *Nano Lett.* **2021**, *21*, 1446–1453.

[19] L. Kang, M. Cui, F. Jiang, Y. Gao, H. Luo, J. Liu, W. Liang, C. Zhi, *Adv. Energy Mater.* **2018**, *8*, 1801090.
[20] Y. Zeng, X. Zhang, R. Qin, X. Liu, P. Fang, D. Zheng, Y. Tong, X. Lu, *Adv. Mater.* **2019**, *31*, 1903675.
[21] J. Y. Kim, G. Liu, G. Y. Shim, H. Kim, J. K. Lee, *Adv. Funct. Mater.* **2020**, *30*, 2004210.
[22] L. Suo, Oleg Borodin, T. Gao, Marco Olguin, Janet Ho, X. Fan, C. Luo, C. Wang, K. Xu, *Science* **2015**, *350*, 938–943.
[23] K. Zhao, C. Wang, Y. Yu, M. Yan, Q. Wei, P. He, Y. Dong, Z. Zhang, X. Wang, L. Mai, *Adv. Mater. Interfaces* **2018**, *5*, 1800848.
[24] M. Zhu, J. Hu, Q. Lu, H. Dong, D. D. Karnaushenko, C. Becker, D. Karnaushenko, Y. Li, H. Tang, Z. Qu, J. Ge, O. G. Schmidt, *Adv. Mater.* **2021**, *33*, 2007497.
[25] S. Guo, L. Qin, T. Zhang, M. Zhou, J. Zhou, G. Fang, S. Liang, *Energy Storage Mater.* **2021**, *34*, 545–562.
[26] S. Wang, Z. Yuan, X. Zhang, S. Bi, Z. Zhou, J. Tian, Q. Zhang, Z. Niu, *Angew. Chem. Int. Ed.* **2021**, *60*, 7056–7060.
[27] Meng, X. Ji, M. Li, T. Liu, W. Dong, Y. Pan, L. Huang, S. Cheng, *Surf. Interfaces* **2022**, *29*, 101782.
[28] L. Li, S. Cheng, L. Deng, T. Liu, W. Dong, Y. Liu, L. Huang, H. Yao, X. Ji, *ACS Appl. Mater. Interfaces* **2023**, *15*, 3953–3960.
[29] Y. Zhang, Y. Liu, Z. Liu, X. Wu, Y. Wen, H. Chen, X. Ni, G. Liu, J. Huang, S. Peng, *J. Energy Chem.* **2022**, *64*, 23–32.
[30] M. Yan, C. Xu, Y. Sun, H. Pan, H. Li, *Nano Energy* **2021**, *82*, 105739.
[31] D. Chao, W. Zhou, C. Ye, Q. Zhang, Y. Chen, L. Gu, K. Davey, S. Z. Qiao, *Angew. Chem. Int. Ed. Engl.* **2019**, *58*, 7823–7828.
[32] L. Deng, M. Wang, X. Ji, S. Cheng, *Ionics* **2020**, *27*, 423–428.

Manuscript received: April 14, 2023
Revised manuscript received: May 18, 2023
Accepted manuscript online: May 19, 2023
Version of record online: June 2, 2023